arXiv:1511.00443v1 [physics.atom-ph] 2 Nov 2015

A simple 2 W continuous-wave laser system for trapping ultracold metastable helium atoms at the 319.8 nm magic wavelength

R.J. Rengelink[1], **R.P.M.J.W. Notermans**[1] **and W. Vassen**[1,*]

[1] *LaserLaB, Department of Physics and Astronomy, Vrije Universiteit Amsterdam, De Boelelaan 1081, 1081 HV Amsterdam, The Netherlands*

[*] *w.vassen@vu.nl*

Abstract: High precision spectroscopy on the $2\ ^3S \rightarrow 2\ ^1S$ transition is possible in ultracold optically trapped helium but the accuracy is limited by the ac-Stark shift induced by the optical dipole trap. To overcome this problem, we have built a trapping laser system at the predicted magic wavelength of 319.8 nm. Our system is based on frequency conversion using commercially available components and produces over 2 W of power at this wavelength. With this system, we show trapping of ultracold atoms, both thermal ($\sim 0.2\ \mu$K) and in a Bose-Einstein condensate, with a trap lifetime of several seconds, mainly limited by off-resonant scattering.

© 2015 Optical Society of America

OCIS codes: (020.7010) Laser trapping; (300.6210) Spectroscopy, atom; (140.3515) Lasers, frequency doubled; (140.3610) Lasers, ultraviolet

References and links

1. A. Antognini *et al.*, "Proton structure from the measurement of 2S-2P transition frequencies of muonic hydrogen," Science **339**(6118), 417-420 (2013).
2. T. Nebel *et al.*, "The Lamb-shift experiment in Muonic helium," Hyperfine interact. **212**(1), 195 (2012).
3. K. Pachucki, and V.A. Yerokhin, "Theory of the helium isotope shift," J. Phys. Chem. Ref. Data **44**, 031205 (2015).
4. P. Cancio Pastor, L. Consolino, G. Giusfredi, P. De Natale, M. Inguscio, V.A. Yerokhin, and K. Pachucki, "Frequency Metrology of Helium around 1083 nm and Determination of the Nuclear Charge Radius," Phys. Rev. Lett. **108**, 143001 (2012).
5. R. van Rooij, J.S. Borbely, J. Simonet, M.D. Hoogerland, K.S.E. Eikema, R.A. Rozendaal, and W. Vassen, "Frequency Metrology in Quantum Degenerate Helium: Direct Measurement of the $2\ ^3S_1 \rightarrow 2\ ^1S_0$ Transition," Science **333**(6039), 196-198 (2011).
6. J. Ye, H.J. Kimble, and H. Katori "Quantum State Engineering and Precision Metrology Using State-Insensitive Light Traps," Science **320**(5884), 1734-1738 (2008).
7. R.P.M.J.W. Notermans, R.J. Rengelink, K.A.H. van Leeuwen, and W. Vassen, "Magic wavelengths for the $2\ ^3S \rightarrow 2\ ^1S$ transition in helium," Phys. Rev. A **90**, 052508 (2014).
8. S. Vasilyev, A. Nevsky, I. Ernsting, M. Hansen, J. Shen, and S. Schiller, "Compact all-solid-state continuous-wave single-frequency UV source with frequency stabilization for laser cooling of Be^+ ions," Appl. Phys. B **103**(1), 27-33 (2011).
9. F.M.J. Cozijn, J. Biesheuvel, A.S. Flores, W. Ubachs, G. Blume, A. Wicht, K. Paschke, G. Erbert, and J.C.J. Koelemeij, "Laser cooling of beryllium ions using a frequency-doubled 626 nm diode laser," Opt. Lett. **38**(13), 2370-2372 (2013).
10. A.C. Wilson, C. Ospelkaus, A.P. VanDevender, J.A. Mlynek, K.R. Brown, D. Leibfried, and D.J. Wineland, "A 750-mW, continuous-wave, solid-state laser source at 313 nm for cooling and manipulating trapped $^9Be^+$ ions," Appl. Phys. B **105**(4), 741-748 (2011).

11. H.-Y. Lo, J. Alonso, D. Kienzler, B.C. Keitch, L.E. de Clercq, V. Negnevitsky, and J.P. Home, "All-solid-state continuous-wave laser systems for ionization, cooling and quantum state manipulation of beryllium ions" Appl. Phys. B **114**(1), 17-25 (2014).
12. J.C.J Koelemeij, W. Hogervorst, and W. Vassen "High-power frequency-stabilized laser for laser cooling of metastable helium at 389 nm" Rev. Sci. Instrum. **76**, 033104 (2005).
13. G.D. Boyd, and D.A. Kleinman "Parametric Interaction of Focused Gaussian Light Beams" J. Appl. Phys. **39**(8), 3597-3639 (1968).
14. O. Gayer, Z. Sacks, E. Galun, and A. Arie, " Temperature and wavelength dependent refractive index equations for MgO-doped congruent and stoichiometric $LiNbO_3$," Appl. Phys. B **91**(2), 343-348 (2008).
15. R. Le Targat, J.-J. Zondy, and P. Lemonde "75%-Efficiency blue generation from an intracavity PPKTP frequency doubler" Opt. Commun. **247**(4-6), 471-481 (2005).
16. K. Simeonidis, TOPTICA Photonics AG, Lochhamer Schlag 19, 82166 Graefelfing, Germany (personal communication, 2014).
17. G. Eaton, CCFE Special Techniques, Culham Science Centre, Abingdon, Oxfordshire, OX14 3DB, UK (personal communication, 2014)
18. A.S. Flores, H.P. Mishra, W. Vassen, and S. Knoop "Simple method for producing Bose-Einstein condensates of metastable helium using a single beam optical dipole trap," arXiv:1508.04019 Appl. Phys. B (to be published)

1. Introduction

The helium atom has proven to be a productive testing ground for fundamental physics. Frequency metrology has been employed as a sensitive test of QED calculations, and also to probe the influence on level energies of the finite size of the nucleus. Such measurements are currently receiving a lot of attention since a measurement of the proton radius in muonic hydrogen found a 7σ discrepancy with the 2010 CODATA value [1]. This discrepancy has been named the "proton radius puzzle", and research is extended to the helium nucleus, with current experiments focussing on the muonic helium ion [2].

In neutral helium, theory and experiment have developed to a level where it is possible to determine the difference in nuclear charge radius between ^{3}He and ^{4}He with high accuracy [3, 4]. One transition very sensitive to the nuclear charge radius is the $2\,^3S \rightarrow 2\,^1S$ transition, which has recently been measured in an ultracold gas trapped in an optical dipole trap (ODT) [5]. This was done both in a Bose-Einstein condensate (BEC) of ^{4}He in the metastable $2\,^3S$ state (^{4}He*) and in a degenerate Fermi gas of ^{3}He*. The 2.3 kHz experimental accuracy of the isotope shift was limited by the ac-Stark shift induced by the ODT. This problem is also encountered in optical lattice clocks where it is solved by employing so-called magic wavelength traps [6]. In a magic wavelength trap, the wavelength of the trapping laser is chosen such that the upper and lower state polarizability are exactly the same, cancelling out the differential ac-Stark shift. For the $2\,^3S$ and $2\,^1S$ levels of helium, we have previously calculated the ac polarizability and compiled a list of magic wavelengths for both isotopes [7]. All useful magic wavelengths are in the ultraviolet spectral region with the most promising candidate located at 319.815 nm for ^{4}He and 319.830 nm for ^{3}He.

Trapping atoms at this wavelength is not straightforward. First of all, to achieve a trap depth comparable to [5], where an infrared ODT at 1557 nm was used, an optical power of approximately 1 W is required. Such powers are not readily available at ultraviolet wavelengths. Secondly, the lifetime of atoms trapped at this magic wavelength is intrinsically limited by two mechanisms: off-resonant excitation to the nearby $2\,^3S \rightarrow 4\,^3P$ transition at 318.9 nm, and two-photon ionization. The total loss rate from these processes should not exceed about 1 s^{-1}, to allow sufficient probe time for spectroscopy.

Considerable progress has been made in the production of laser light at the nearby wavelength of 313 nm, for the purpose of laser cooling Be^+ ions [8, 9, 10, 11]. High power (750 mW) was generated by sum frequency mixing and subsequent frequency doubling of two fiber lasers, retaining most of their high spatial and spectral mode quality [10]. More recently, production of up to 2 W was demonstrated with such a scheme [11].

In section 2, we demonstrate a laser system producing over 2 W at 319.8 nm based on a modification of this scheme. Our system is built out of commercially available components which makes it simple, compact, and reliable. In section 3 we show that our source can be used to trap helium atoms with an acceptable lifetime of a few seconds, such that spectroscopy on the $2\,^3S \rightarrow 2\,^1S$ transition can be performed.

2. Laser System

The system can be divided in a sum frequency generation (SFG) part, which generates 639.6 nm light from two infrared lasers, and a second harmonic generation (SHG) part which frequency doubles the SFG light to 319.8 nm. In the following, we will first give a full overview of the optical system before discussing the results and performance of the SFG and SHG parts separately.

2.1. Overview

Figure 1 shows a schematic overview of the optical setup. The setup is relatively compact with all of the components, except for the lasers and the control electronics, mounted on a single 1000×500 mm^2 optical breadboard. The system starts with two fiber lasers (NKT photonics Koheras Adjustik E15 and Y10) with center wavelengths of 1557.28 nm and 1085.45 nm. The thermal tuning ranges are 1000 pm and 700 pm respectively, covering a spectral range much larger than the uncertainty in the calculated magic wavelength. The lasers seed two 10 W fiber amplifiers (NuFern NUA-1084-PB-0010-C2 and NUA-1550-PB-0010-C2), with isolated polarization maintaining free-space output couplers. The beams are separately focussed to achieve optimal sum frequency generation.

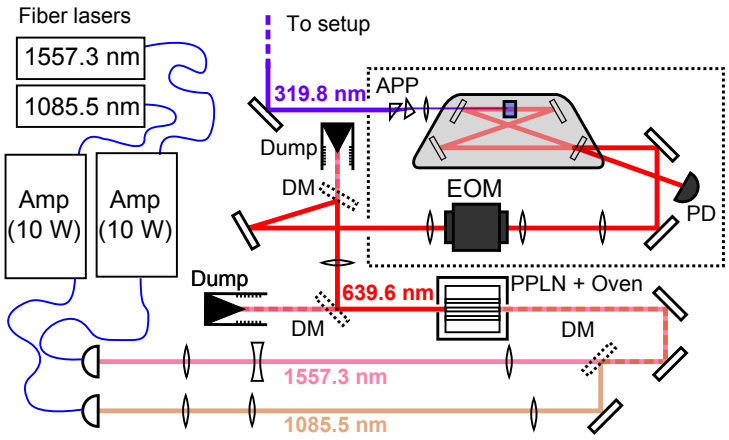

Fig. 1. Schematic view of the UV laser system. Two infrared fiber lasers at 1085.5 nm and 1557.3 nm seed two 10 W amplifiers. The infrared beams are independently focussed, and overlapped on a dichroic mirror (DM). The combined beam passes through a temperature stabilized PPLN crystal. More dichroic mirrors filter residual infrared light from the SFG beam at 639.6 nm. This beam is mode-matched and phase modulated by a 2 MHz electro-optic modulator (EOM) and the cavity reflection is monitored using a photodiode (PD) to allow Pound-Drever-Hall locking of the cavity. The final UV output beam is then collimated and ellipticity is compensated by an anamorphic prism pair (APP).

The output beams are to an excellent degree of approximation Gaussian, and can be described completely by two parameters: their (minimum) waist size (w_0), which is directly related to

their Rayleigh range ($z_R = \pi w_0^2/\lambda$), and the position of their focus. In order to achieve optimal conversion these parameters must be matched both to each other and to the crystal. Achieving this condition is not entirely straightforward because of the coupled nature of the problem.

We first collimate the 1557.3 nm beam with an $f = 300$ mm lens, and then focus by two lenses with focal distances of -100 mm and 200 mm. The beam waist can now be changed by moving either of the focussing lenses, but doing so will also move the focal point. The 1085.5 nm beam is first passed through a telescope consisting of two lenses with focal distances of 200 mm and 50 mm and is then focussed by an $f = 300$ mm lens. The focal point can be changed without affecting the waist size by moving the focussing lens. In this way, the foci of the beams are matched by first setting the waist of the 1085.5 nm beam to the desired focussing, secondly matching the 1557.3 nm beam waist to it, and finally overlapping the focal point of the 1085.5 nm beam with that of the 1557.3 nm beam.

With fixed beam parameters, the infrared beams are overlapped on a dichroic mirror and passed through a 40 mm MgO doped periodically poled lithium niobate (PPLN) crystal (Covesion) with a poling period of 12.1μm. The crystal is mounted in an oven and temperature stabilized at $\sim 90^\circ$C. The output beam from the crystal contains both the sum frequency and residual infrared light. This residual light is filtered from the beam by two dichroic mirrors and the SFG beam is collimated by a $f = 250$ mm lens to a waist of ~ 1 mm.

The light is then coupled (free-space) into a commercial frequency doubling system (Toptica SHG pro) where it is mode-matched to the cavity and passed through an electro-optical modulator (EOM). The EOM modulates 2 MHz sidebands on the laser carrier frequency to allow Pound-Drever-Hall locking of the cavity. The doubling cavity is similar to [12], the main differences being the locking scheme (Pound-Drever-Hall instead of Hänsch-Couillaud) and the crystal (AR-coated rather than Brewster cut). The UV output is collimated and passed through an anamorphic prism pair to reduce beam ellipticity.

2.2. Sum Frequency Generation

The purpose of the SFG stage is to convert the available infrared laser light into useful SFG light with high efficiency. To achieve this it is necessary to focus the input beams tightly so that a high peak intensity is reached, but not so tightly that the beams diverge too quickly before they reach the end of the crystal. As described by Boyd and Kleinman [13], this process can be optimized with respect to the dimensionless focussing parameter $\xi = l/2z_R$, which is the ratio of the crystal length l to the confocal parameter of the beam (twice the Rayleigh length z_R). Although optimal at $\xi \approx 2.84$, the efficiency varies quite slowly so that at confocal focussing ($\xi = 1$) it is still approximately 80% of its maximum value. The system produces more power than required and the confocal condition is chosen because of practical considerations such as the available path length and the size of the entrance surface of the crystal.

The infrared beams were set to the confocal condition as described in section 2.1. The waist sizes are measured to be $56(1)$ μm ($z_R = 8.9(3)$ mm) for the 1085.5 nm beam and $63(1)$ μm ($z_R = 7.9(3)$ mm) for the 1557.3 nm beam, with their waist positions located within 1 mm of each other. By correcting for the refractive index of the crystals, which can be calculated based on known Sellmeier coefficients [14], the focussing parameter inside the crystal is found to be $\xi = 1.03$ for the 1085.5 nm beam and $\xi = 1.16$ for the 1557.3 nm beam.

Figure 2a shows the converted power as a function of the product of the input powers (input power product, IPP). When different combinations of input powers with equal IPP are used they produce almost the same SFG output power. This can be seen more clearly in a contour plot of the output power as a function of input powers (figure 2b, based on a linear interpolation of the same dataset) where contours of constant IPP follow constant output power. From this we conclude that the total converted power is a function of IPP only, and does not depend on

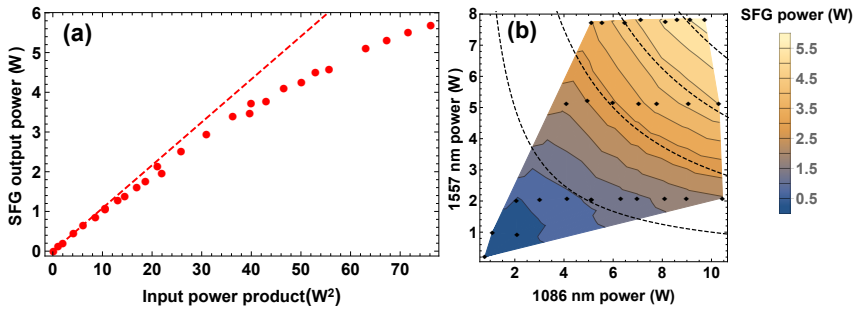

Fig. 2. Results of sum frequency generation. (a) Sum frequency power as a function of the input power product (IPP) of the infrared lasers. The dashed line is a linear fit at low input powers (slope 0.108(1) W^{-1}). (b) Contourplot of the sum frequency power as a function of both input powers, based on a linear interpolation of the same dataset as (a). Black diamonds indicate measured datapoints, the dashed lines indicate contours of constant IPP.

the exact composition of infrared powers.

In order to achieve the power conversion plotted in Figs. 2a and 2b, it is necessary to optimize for crystal temperature at each input power product. The reason for this is shown in Figure 3, which shows the conversion efficiency as a function of crystal temperature at different input powers. As the input power becomes higher, the optimal temperature shifts to lower temperature and the crystal temperature needs to be adjusted to achieve maximum conversion. A possible explanation for this behaviour is that light is absorbed in the center of the crystal and heats it locally. This causes a slightly elevated temperature, and consequently imperfect phase matching at the center of the crystal (where conversion occurs) compared to the crystal edge (with respect to which the temperature is controlled). This effect is compensated when the crystal temperature is set to a slightly lower temperature.

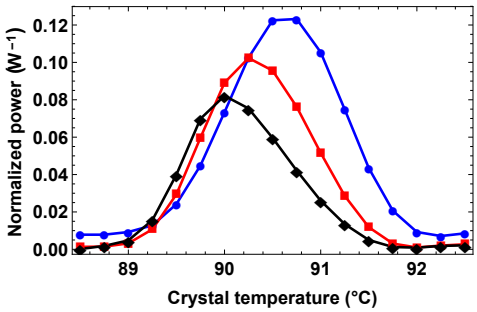

Fig. 3. Sum frequency production as a function of crystal temperature, normalized for measured input power product. The plot shows input power products of 1.4 W^2 (blue circles), 35.7 W^2 (red squares), and 78.0 W^2 (black diamonds). At higher input powers the temperature graph becomes slanted towards lower temperature, indicating thermal effects.

At low input powers the SHG output power scales linearly with a slope of 0.108(1) W^{-1}, comparable to other experiments using a similar crystal [10, 11]. At higher output powers a deviation from the linear behaviour is seen. This may be a left-over thermal effect, or it may be that, because of the high conversion efficiency, pump depletion needs to be taken into account. At an IPP of 80 W^2, consisting of 8 W at 1557.3 nm and 10 W at 1085.5 nm, a maximum output power of almost 6 W of SFG light is produced, which corresponds to a conversion efficiency of

33%.

2.3. *Second Harmonic Generation*

With the generated SFG light, the Toptica SHG pro system is pumped. Using a commercial frequency doubling system has the advantages of reliability and stability but a downside is that some system parameters are not disclosed. We will therefore describe the system as a whole with reported in- and output powers measured before and after the full system.

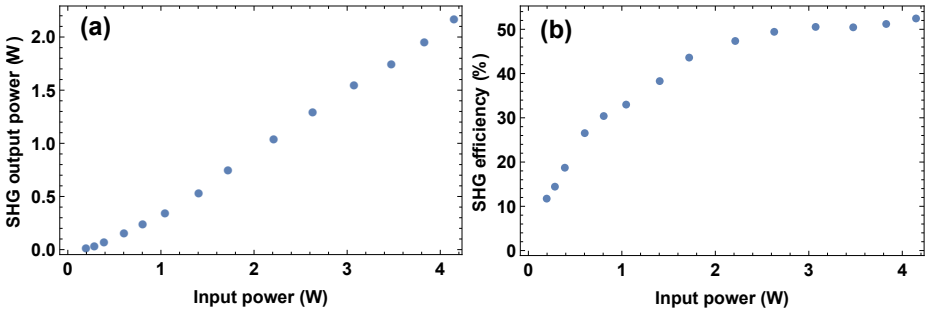

Fig. 4. Results from the SHG system. (a) UV output power (319.8 nm) as a function of total input power (639.6 nm) going into the full system. The output increases quadratically at low input powers, but saturates to a linear asymptote at higher powers. (b) System conversion efficiency (ratio of total input and output power) as a function of input power. The efficiency saturates at ∼50%.

Figure 4 shows the system output power and conversion efficiency of the SHG section. At an input power of ∼2 W the conversion efficiency saturates at about 50% and at an input power of 4 W a maximum output power of more than 2 W of UV light was achieved. At this point the cavity coupling efficiency is just over 80%. This behaviour is qualitatively similar to what is observed in other SHG systems [12, 15]. Although more SFG input power is available, we choose to remain below 4 W input power as the system is already operating close to the (UV induced) damage threshold of the crystal at these powers [16]. Peak-to-peak UV intensity fluctuations of 4% were measured over a 4 hour period. This is within the specifications for intensity noise of the fiber amplifiers.

The beam profile of the cavity output is still Gaussian, but shows ellipticity due to crystal walk-off. Directly from the cavity we observe a beam waist of ~ 0.7 mm in the vertical and ~ 0.1 mm in the horizontal direction. This beam is passed through a collimating lens and an anamorphic prism pair to produce a more circular beam. We measure the final beam waist of $\sim 0.21 \times 0.35$ mm^2. Despite the modest ellipticity these beam parameters still allow tight focussing, an essential requirement for optical dipole trapping.

3. Trapping

Now that we are able to produce sufficient power at 319.8 nm, we implement the laser system into our existing setup to demonstrate trapping and to characterize the trap lifetime. We prepare the beam for trapping by enlarging it with a 1:2 telescope and focus it inside the vacuum chamber with an $f = 400$ mm lens to a waist of $w_0^{(1)} \times w_0^{(2)} = 64.3(1.0) \times 55.6(7)$ μm^2. The focus positions along the horizontal and vertical axes are found to lie 12(2) mm apart which is small compared to the Rayleigh lengths (40.0(6) mm and 30.0(4) mm). We measure 62% total transmission of the two windows of the vacuum chamber. While high, these losses are expected from uncoated sapphire vacuum windows [17].

A transmission per window of $T_1 = \sqrt{0.62} \approx 0.78$ is assumed to estimate the power inside the vacuum chamber. Therefore, at a power (P) of 1 W and neglecting astigmatism, the beam has peak intensity

$$I_p = \frac{2T_1 P}{\pi w_0^{(1)} w_0^{(2)}} = 14 \text{ kWcm}^{-2}. \quad (1)$$

Based on the polarizability (calculated in [7]) this translates to a trap depth of $\sim 6.0\ \mu\text{K W}^{-1}$ for a single beam. The trap depth of our ODT is therefore far below the recoil temperature

$$T_{rec} = \frac{\hbar^2 k^2}{k_B m} = 46.7\ \mu\text{K}, \quad (2)$$

where $k = 2\pi/\lambda$ is the photon wavenumber and m is the atomic mass of helium. We can therefore safely assume that each photon scattering event leads to the loss of the scattered atom. Additionally, the excess energy of the scattered atom can heat the other atoms or even kick more atoms out of the trap.

When two- and three-body losses can be neglected, the total loss rate is a combination of three distinct rates: a background loss rate R_{bg} due to the background pressure inside the chamber, a loss rate R_{sc} due to photon scattering, and a loss rate R_{ion} due to two-photon ionization. These mechanisms scale in different ways with ODT power. The total loss rate is

$$R_{tot} = R_{bg} + R_{sc} I_p + R_{ion} I_p^2. \quad (3)$$

The Rayleigh length of the focussed UV beam is comparable to the $\sim$4 cm spacing between the vacuum windows. Therefore, in a single beam ODT trapped atoms are able to collide with the windows and leave the trap. To avoid this some means of axial confinement is necessary. We use two different methods to provide this confinement. The first is to add a magnetic field gradient along the beam direction to create a hybrid trap [18]. With this method the loss rate and trap depth are straightforward to interpret. However, peak densities are not high enough to produce a BEC. The other method is to create a two-colour crossed-beam ODT using the UV beam and additionally a focussed 1557 nm beam which was already in place [5]. This trap gives a high enough peak density for a BEC to form.

3.1. Hybrid Trap

We prepare an ultracold sample in a way previously described [5]. A beam of He^* atoms is generated from a liquid nitrogen cooled dc-discharge, collimated, slowed in a Zeeman slower, and captured in a magneto-optical trap. Here the atoms are cooled to approximately 0.5 mK. Subsequently they are spin-polarized, loaded into a Ioffe-Pritchard type magnetic trap and Doppler cooled to approximately 130 μK. Finally, the atoms are cooled to $\sim 0.2\ \mu$K by forced rf evaporative cooling inside the magnetic trap.

The cloud is transferred to the hybrid trap consisting of the UV beam and a quadrupole magnetic trap (QMT) generated by a set of QMT coils in anti-Helmholtz configuration. Figure 5 shows a schematic of this trap. The quadrupole field has a strong axis gradient of 0.54 Gauss/cm but gravity acts in a direction perpendicular to this axis. In this direction the gradient is only half the magnitude which is well below the leviation gradient of $mg/\mu = 0.351$ Gauss/cm [18]. Below this gradient gravity is stronger than the confining magnetic force so that atoms are not trapped in the absence of the UV beam. The QMT therefore adds confinement but does not contribute to the trap depth. A homogeneous magnetic field is applied with a set of fine-tune coils to minimize trap oscillations induced by the loading step.

The atoms are detected either by absorption imaging or by a micro-channel plate detector (MCP) located 17 cm below the trap center. MCP time of flight measurements are done as a

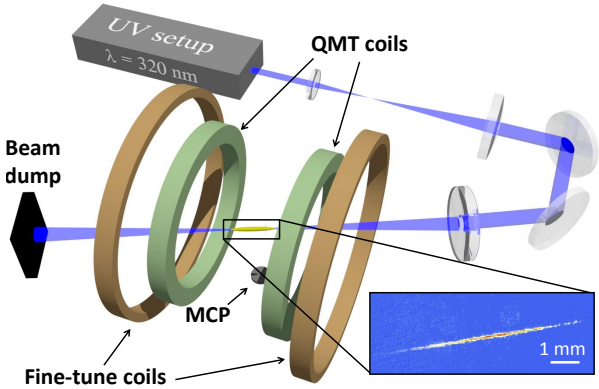

Fig. 5. Schematic view of the hybrid trap geometry. Atoms are trapped by the combination of the UV-laser beam and the quadrupole magnetic trap (QMT) coils. A set of fine-tune coils allows precise tuning of the trap center. Because of limited optical access the UV laser beam is at an angle of $\sim 9.5^\circ$ with the magnetic field axis. High-resolution detection is done using a micro-channel plate detector (MCP). Inset: in-situ absorption image of atoms in the UV hybrid trap.

function of hold time in the hybrid trap. The time of flight signals are fitted with a thermal Bose-Einstein distribution to extract the temperature of the gas as well as the atom number. The decay in atom number is fitted with an exponential (with an oscillating component to account for residual trap oscillations). The first few seconds of the decay are not fitted to neglect two-body loss and thermalization effects.

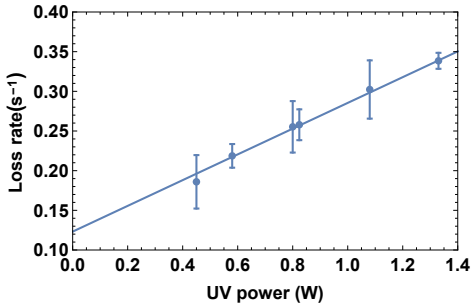

Fig. 6. Hybrid trap one-body loss rate as a function of UV power. The blue line is a linear fit with a slope of 0.16(2) $s^{-1}W^{-1}$, corresponding to off-resonant scattering.

Figure 6 shows the loss rate of a thermal gas inside the hybrid trap. The loss rate varies linearly with power, which is consistent with only background collisions and off-resonant scattering; two-photon ionization would depend quadratically on power. A linear fit gives a slope of about 0.16(2) $s^{-1}W^{-1}$ ($R_{sc} \approx 1.2$ $s^{-1}W^{-1}m^2$, see equation 3), with a background loss rate of 0.12(2) s^{-1}. This background loss rate is consistent with the loss rate of 0.13(1) s^{-1} in a hybrid trap of comparable depth using our 1557 nm ODT for which off-resonant scattering is negligible [7]. Figure 7 shows the fitted temperature as a function of hold time in the hybrid trap. This temperature is not constant; after a quick thermalization the cloud starts heating up. This heating may be caused by scattered atoms dumping a small portion of their high recoil

energy in the atomic cloud. In principle it is also possible that a scattered atom is able to dump all of its energy in the cloud and thermalize instead of leaving the trap. At the highest observed heating rate $\dot{T} \approx 0.04\ \mu\mathrm{K\ s^{-1}}$, this contributes no more than $\dot{T}/T_{rec} \approx 0.001\mathrm{s^{-1}}$ to the loss rate, negligible compared to other processes.

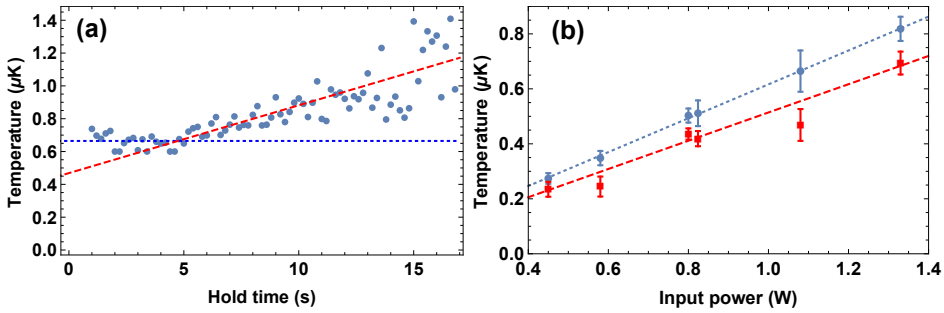

Fig. 7. (a) Temperature as a function of hold time in the hybrid trap. After some thermalization time the atomic cloud starts to heat as a result of UV absorption. The blue dotted line is a constant fit to the temperature around the minimum to extract the minimum temperature. The red dashed line is a linear fit to the temperature after a few seconds to extract the heating rate. (b) Determination of the trap temperature based on minimum temperature (blue circles), and an extrapolation to zero hold time of the heating rate (red squares). From linear fits to these data an upper (lower) bound is set on the temperature in absence of heating of $0.62(2)\ \mu\mathrm{K\ W^{-1}}$ ($0.51(2)\ \mu\mathrm{K\ W^{-1}}$).

To give an estimate of the equilibrium temperature inside the trap (in the absence of scattering) we take the minimum achieved temperature as an upper bound, and a linear extrapolation of the heating to zero hold time as a lower bound. In this way we extract temperatures of $0.62(2)\ \mu\mathrm{K\ W^{-1}}$ and $0.51(2)\ \mu\mathrm{K\ W^{-1}}$ respectively. This is approximately a factor 10 lower than the calculated trap depth and corresponds to a truncation parameter $\eta = 10$ which is typically found in a thermalized trapped gas [18].

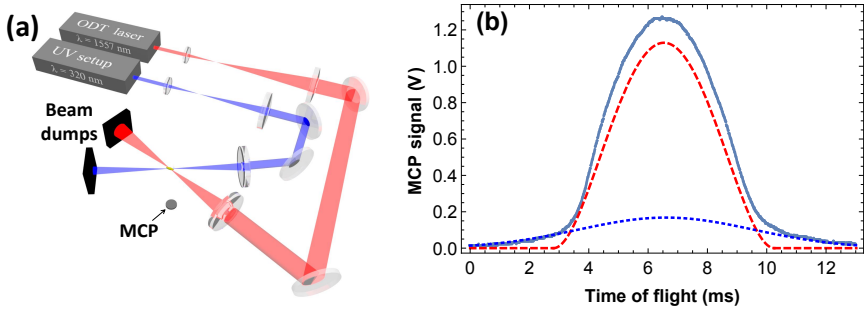

Fig. 8. (a) Schematic picture of the two-colour ODT setup. The angle between the beams is 19°. (b) MCP time-of-flight measurement of a BEC in a two colour optical dipole trap. The signal is fit with a bimodal distribution indicating a BEC (red dashed line) and a thermal fraction (blue dotted line).

3.2. Two-colour Trap

Because of the low confinement provided by the hybrid trap, no BEC was observed. To provide enough confinement to observe BEC we switch to a two-colour trap consisting of the UV beam

and an IR beam (focussed to a waist of 85 μm) which cross at an angle of 19°. Figure 8a shows a schematic of the setup. Figure 8b shows the corresponding time-of flight signal on the MCP, fit with a bimodal distribution. Superposed on the thermal distribution is a clear inverted parabola Thomas-Fermi profile demonstrating Bose-Einstein condensation. For this BEC a one-body lifetime is observed of $\sim 4s$.

4. Conclusion

In order to perform magic wavelength trapping of metastable helium atoms we have realized a laser system which produces over 2 W at 319.8 nm, with not yet an indication of a reduction of SHG efficiency at higher pump power. The setup is built from commercially available fiber lasers, amplifiers and SFG/SHG components. The produced UV light is used to trap an ultracold (~ 0.2 μK) thermal gas in a hybrid trap and a BEC in a two colour ODT. Trap losses are found to be mainly due to off-resonant scattering with a rate of 0.16(2) s^{-1} W^{-1}.

With this system we can make a sufficiently deep dipole trap in the UV while keeping the intrinsic losses at an acceptable level such that spectroscopy is possible. This opens the door to a full magic wavelength ODT and a more precise measurement of the $2\ ^3S \rightarrow 2\ ^1S$ transition frequency.

Acknowledgments

We would like to thank Christian Rahlff of Covesion for useful comments about the PPLN crystal, Steven Knoop for useful discussions about hybrid trapping and Rob Kortekaas for technical support. This work is part of the research programme of the Foundation for Fundamental Research on Matter (FOM), which is part of the Netherlands Organisation for Scientific Research (NWO).